Alicja Krella
Institute of Fluid-Flow Machinery, Polish Academy of Sciences, Poland

Andrzej Zieliński
Faculty of Mechanical Engineering, Technical University of Gdańsk, Poland

CHARACTERISTICS OF THE INCUBATION PERIOD OF THE CAVITATION EROSION OF ALUMINIUM-MAGNESIUM ALLOY PA2

ABSTRACT

The cavitation attack can cause various damages of the material, depending on cavitation intensity. Herein the relationships between cavitation intensity and the changes of microstructure of aluminium-magnesium alloy are presented. Correlation between energy flux density and mass erosion rate is described by simple empirical mathematical expression:

$$ER = 1E - 05\ J^2 + 0{,}0005\ J,$$

where:

    J   – energy flux density,
    ER – cavitation erosion rate.

Here it is shown that for the intensity of cavitation $J \leq 1$ mW/m^2 the duration of the incubation period is invariable, while at the cavitation intensity $J > 1$ mW/m^2 its duration decreases with increasing energy flux density J.

INTRODUCTION

Cavitation is a process in which the bubbles, consisting of vapour or gas, expand and collapse depending on the surrounding pressure, which decreases and increases rapidly [1–3]. The internal phenomena such as the thermal diffusion, the diffusion of vapour and gas, the mist formation due to the homogeneous condensation and the heat and mass transfer through bubble wall, have significant influence on the cavitation process. The cavitation phenomenon may cause serious change in microstructure and intrinsic stress level of the material. Macroscopically, the change in hardness is often observed; microscopically, the slip bands and deformation twins appear, and the phase transformations may occur in unstable alloys [4–6].

The energy E_a absorbed by the volume of the material fractured is given by [7]:

$$E_a = \Delta V \cdot S_e \qquad (1)$$

where E_a is the energy absorbed by eroded material, ΔV is the volume of the eroded material and S_e stands for an erosion strength which represents the energy – absorbing capacity of the material per unit volume under action of the erosive forces.

The energy flux density J determined by implosion of cavitation microbubbles may be calculated from the following expression [8]:

$$J = \frac{1}{T} \cdot \frac{1}{2\rho c_s} \sum_{k=1}^{M} n_k p_k^2 \qquad (2)$$

where:
- T – denotes duration of the pressure pulses sampling period,
- ρ – liquid density,
- c – sound velocity in liquid,
- M – number of pressure intervals,
- n_k – number of pulses in a single interval,
- p_k – value of pressure amplitude in the *k*-th interval.

The cavitation process is divided into 3 stages: incubation, acceleration and steady state period. The most important for the majority of industrial equipment is the incubation period. The cavitation damage process begins when the cavitation pits and cracks on the surface are formed, then the pits and cracks enlarge, inside metal arise slip bands, twinning occurs and finally the stepwise propagation of the pits and cracks results in the mass loss.

In [9–11] the relationships between the number of pits and the size of pits at different flow conditions were presented. When cavitation intensity rises the number of small and large pits rises, too. It was stated in [12] that the ratio of the increment rates of pits of different size could an indicator of the hardening of the material. As shown in [13], the number of pits developed during the erosion test is not a simple function of the energy flux density, but it may be related to different dynamics of cavitation cloud at different cavitation intensity.

The objective of this paper is to search for relationship between mass erosion rate, duration of incubation period, changes of microhardness during incubation period and microstructural change in the AlMg2 alloy and at different density of the energy flux delivered to the material by imploding cavities.

EXPERIMENTAL

The research tests were performed in the Erdmann-Jesnitzer type cavitation tunnel at the laboratory of the Institute of Fluid–Flow Machinery, Polish Academy of Sciences, Gdańsk, Poland (Fig. 1). The Erdmann-Jesnitzer test chamber enables to study erosion damage in different areas of cavitation cloud and at different cavitation intensities. The inlet and outlet pressure, the distance between the barricades and the position of the specimen can be adjusted. The cavities (cavitating vortices and bubbles) are generated due to the pressure decrease in the slot between two cylindrical barricades. Perspex windows on both sides of the chamber enable observation of the cavitation cloud fluctuations.

The Al-Mg alloy of chemical composition: 97.7% Al and 2.3% Mg was investigated. The mechanical properties were determined as: tensile strength 230 MPa, elongation $\varepsilon = 15\%$ [14].

The tested aluminium alloy is a plastic material with high energy of location faults, high inclination for transversal slips and screw dislocations. These properties are linked to small value of tangential stress needed to produce plastic strain. Approximate value of this stress is comprised within the 1÷2 MPa range [15]. Therefore, cavitation pulses of lower collapse pressure are not able to produce even a plastic deformation.

Specimens (five specimens were put together in cavitation chamber) were subjected to cavitation impingement at inlet pressure $p_1 = 1200$ kPa, outlet pressure $p_2 = 130$ kPa and 5 mm slot width, and at inlet pressure $p_1 = 1000$ kPa, outlet pressure $p_2 = 130$ kPa and 5 mm slot width. The specimens together had dimensions $80 \times 45 \times 16$ mm.
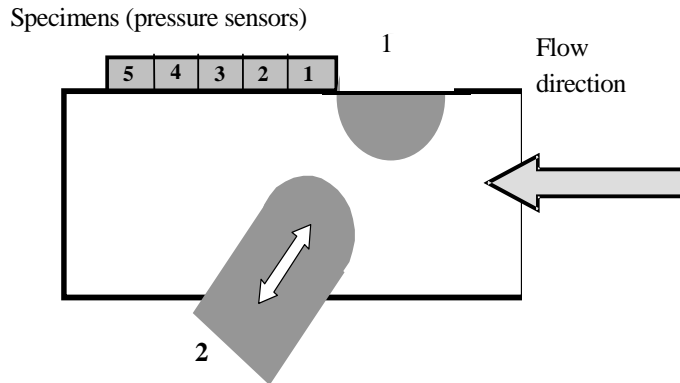
Fig. 1. Schematic of the Erdmann-Jesnitzer type cavitation chamber: 1 – barricade, 2 – counter-barricade. The width of the slot between the barricades can be adjusted within the $0 \div 15$ mm range

The values of energy flux density J at test conditions, calculated on the base of expression (2) are shown in Table 1. The most intensive pulses were formed at the shortest distance from the slot – 7 mm, that is for specimen No 1.

Table 1. *The energy flux density calculated for performed tests*

Pressure in front of/behind the chamber; slot width	Energy flux density at different distance from the slot, $J \times 10^{-3}$ Wm^{-2}				
	7 mm	21 mm	35 mm	49 mm	64 mm
1000/130 kPa; 5 mm	10.93	5.13	0.026	0.068	0.724
1200/130 kPa; 5 mm	18.85	9.56	0.024	0.083	1.3

The mass loss was determined by the weight technique. The dislocation structure was examined by the transmission electron microscopes Jeol JEM 100B and JEM 3010 at the Warsaw University of Technology.

RESULTS

The erosion curves of aluminium-magnesium alloy are shown in Figs. 2 and 3.

As seen the erosion increases with increasing energy flux density J. The erosion was the highest for the energy flux density $J = 18.85$ mW/m^2. In this case, the mass loss after 11 hours of exposure equalled 0.09 g (Fig. 3). The weight of the material removed after 11 hours exposure at $J = 10.93$ mW/m^2 equalled 0.0485 g (Fig. 2). On the rest specimens, where $J \le 1$ mW/m^2, the mass losses were nearly the same and equalled only 0.0005 g after the test.
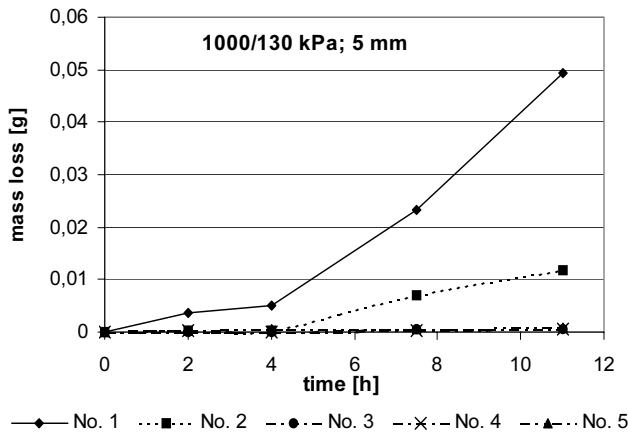
Fig. 2. Erosion curves of aluminium – magnesium alloy after 10 hours of exposure at inlet pressure p_1 = 1000 kPa, outlet pressure p_2 = 130 kPa and 5 mm slot width
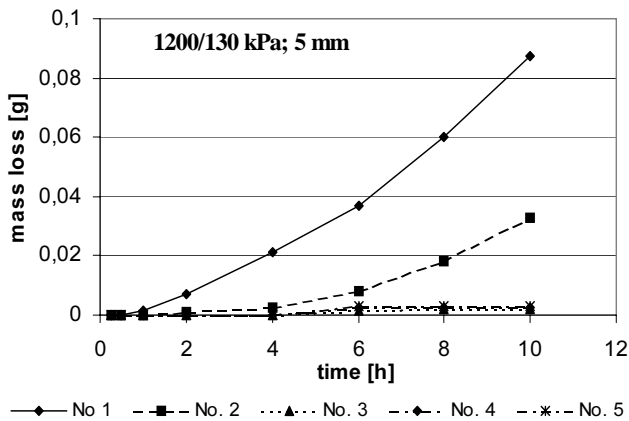
Fig. 3. Erosion curves of aluminium – magnesium alloy after 11 hours of exposure at inlet pressure p_1 = 1200 kPa, outlet pressure p_2 = 130 kPa and 5 mm slot width

Tracing the dependence of the duration of the incubation period on the energy flux density J (Fig. 4.), one can see that at $J \leq 1$ mW/m^2 the incubation period duration is invariable, while at $J > 1$ mW/m^2 it decreases with an increasing energy flux density J.

It can be inferred from Fig. 5, that there exists a parabolic relationship between the energy flux density parameter J and the erosion rate ER. At $J \leq 1$ mW/m^2 cavitation erosion rate is nearly zero. Up from this value it rapidly increases with the growth of the energy flux density parameter J. There is satisfactory correlation between energy flux density and the mass erosion rate, which may be described by a simple empirical mathematical expression:

$$ER = 1E - 05\,J^2 + 0{,}0005\,J,$$

where:

    J   – energy flux density,
    ER – cavitation erosion rate.
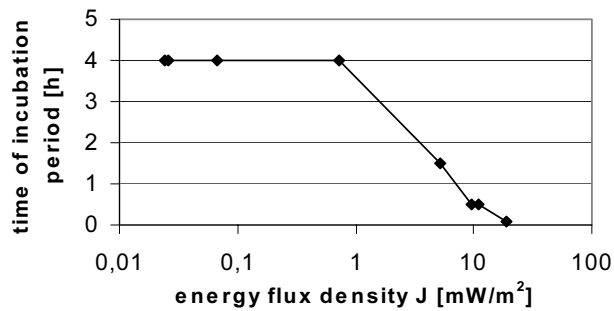
Fig. 4. Relationship be77ween duration of incubation period and an energy flux density J
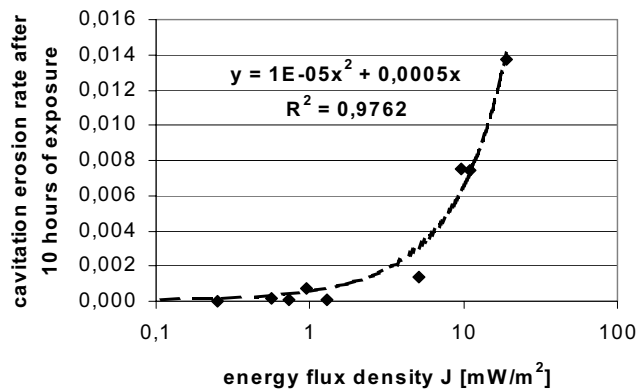
Fig. 5. Relationship between the energy flux density parameter J and the erosion rate determined for all specimens

Development of cavitation pits on the Al alloy specimen of 80×45 mm size in the initial (incubation) cavitation erosion stage at $p_1 = 1000$ kPa and $p_2 = 120$ kPa pressures ware analysed from the places of pressure sensors (Fig. 8). The alloy was subjected to four consecutive exposures, each of 85 s duration. After each exposure, examinations with the light microscope were carried out at magnification of 75×. The pits of over 20 μm in diameter generally prevailed. The state of the surface subjected to cavitation, as well as the shape and size of indentations in the material due to collapsing cavities are depicted in Fig. 6. It is worthwhile to notice that the indentation shown in Photo 2 seems to contain only a single pit when observed at magnification 75× (Fig. 7a). However, at magnification 150× one can easily discern two independent deformations, situated close to each other (Fig. 7b). Pits formed by collapsing bubbles are featured by a characteristic ring shape with the undamaged central area (Fig. 6 – arrows). Such shape is typical for collisions of small liquid jets with a solid.

By plotting the number of counted pits after 255 s and 315 s of exposure versus density of the energy flux delivered to the material, one receives the diagram shown in Fig. 6. The average increment of the number of pits after every exposure was about 40%, for higher cavitation intensities ($J = 10.56 \times 10^{-3}$ W/m^2) this increment was as large as 60%. One should keep in mind that the counted number of pits is underestimated and the realistic increment of the number of pits is higher than that given in Fig. 6. Adopting a logarithmic scale for the number of

indentations one yields a linear dependence, which proves good correlation between the number of pits and the energy flux density.
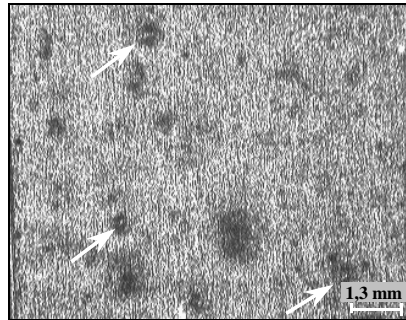
Fig. 6. Image of the surface after 315s of exposure at intensity equal $J = 10.93$ mW/m^2
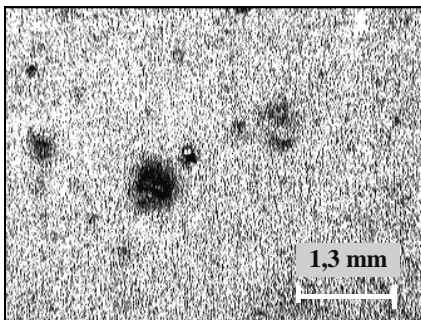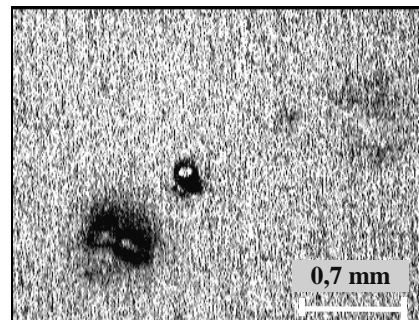
a)   b)

Fig. 7. The shapes of an indentation consisting of two traces of cavitation bubbles collapse at intensity equal
$J = 10.93$ mW/m^2

The results of microhardness measurements are shown in Figs. 7-9. The microhardness was measured beneath exposed surface at constant distance of 0.02 and 0.2 mm at every minute during the first three minutes of incubation period.

There high increase of microhardness at 0.02 mm underneath at the beginning of incubation period at the cavitation intensity $J = 10.93$ mW/m^2 occurred (Fig. 9). After 1 minute of exposure the microhardness increased over 34%, and after 3 minutes –70%. Microhardness at 0.2 mm underneath at the beginning slightly increased, and later decreased below the initial value.
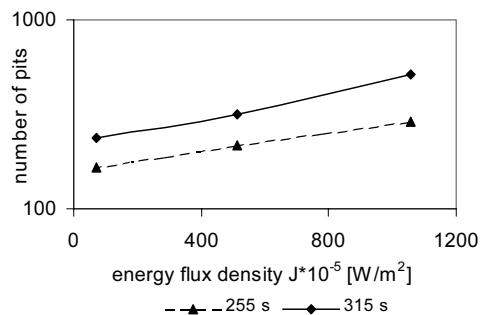
Fig. 8. Relationship of number of pits depending on energy flux density J at inlet pressure $p_1 = 1000$ kPa, outlet pressure
$p_2 = 130$ kPa and 5 mm slot width
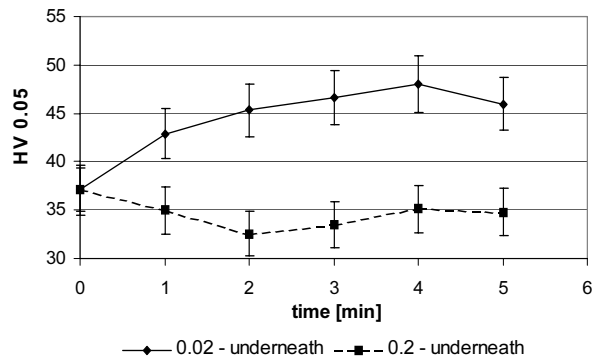
Fig. 9. Change of microhardness during cavitation test at cavitation intensity J = 10.93 mW/m^2

At the energy flux density J = 5.13 mW/m^2 or less (Figs. 10, 11), the microhardness decreased reaching the lowest value after 1 minute of exposure.

At cavitation intensity J = 5.13 mW/m^2 the microhardness decreased 8% after 1 minute of exposure (Fig. 10). During the second minute of cavitation the microhardness increased to initial value, and later on – during next minute of exposure – it increased over 27%. The microhardness curve at 0.2 mm under the surface has the shape similar to that observed at 0.02 mm underneath. After 1 minute of exposure the microhardness decreased 18%, afterwards increased slightly, but not exceeding the initial value.
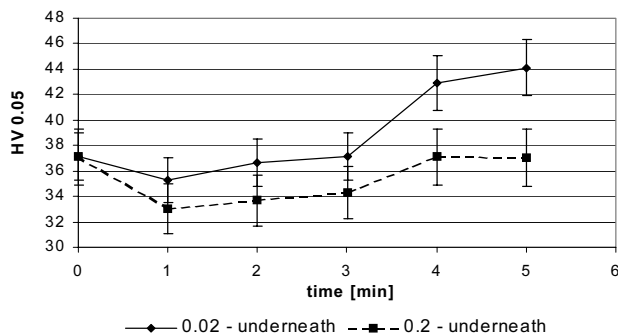
Fig. 10. Change of microhardness during cavitation test at cavitation intensity J = 5.13 mW/m^2
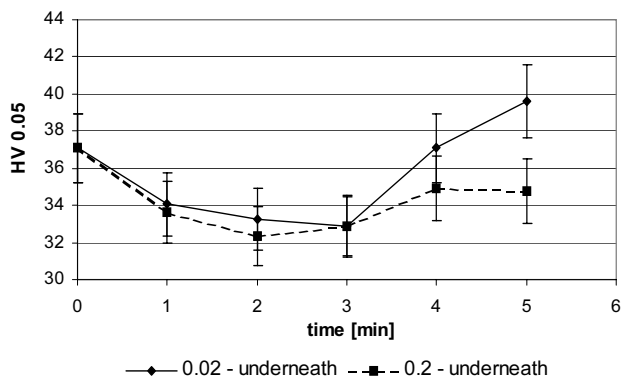
Fig. 11. Change of microhardness during cavitation test at cavitation intensity J = 0.026 mW/m^2

In the case of low cavitation intensities the microhardness decreased reaching the lowest value after 1 minute of exposure (Fig. 9). The downfall of microhardness was about 20% at 0.02 mm under the surface and 25% at 0.2 mm under the surface. The microhardness didn't increase to initial value during the first three minutes of exposure.

The results of the examinations of the microstructure involving dislocation network are shown in Figs. 12–16.

In the high intensity zone ($J = 10.93$ mW/m^2) dense dislocation network with some precipitates and nano-precipitates was detected. Cellular dislocation structure typical for deformation rate, at which the dislocations can't move and they are blocked, was also observed (Fig. 12 and 13).
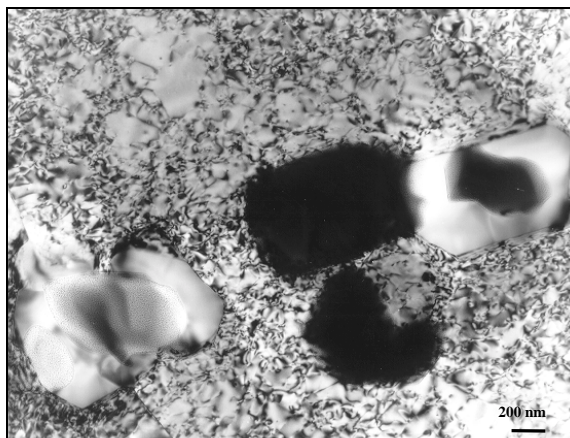
Fig. 12. Precipitates in nanostructure at intensity equal $J = 10.93$ mW/m^2
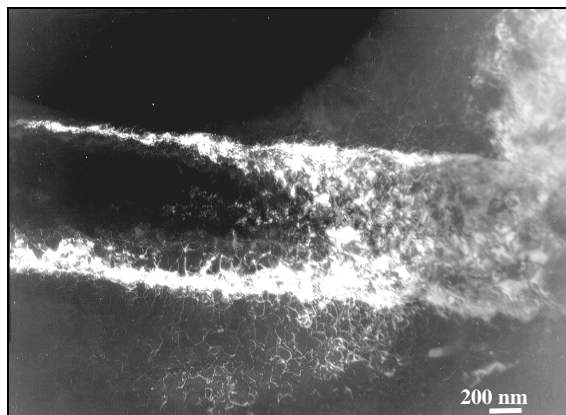
Fig. 13. Three-dimensional tunnel at intensity equal $J = 10.93$ mW/m^2

Fig. 12 shows tough precipitates or inclusions subjected to action of collapsing bubbles. The surface of precipitate was relatively resistant to the cavitation strike but in two areas the appearance of a great number of very small pits may be observed. The bright precipitate laying on the grain boundaries looks like original precipitate, whiles the black one seems to grow as a result of derivative effect of cavitation action. The precipitates have typical shape of HZ crystal lattice.

Effect of three-dimensional dislocation structure is shown on Fig. 13. Three-dimensional tunnel stood for its broadened grain boundary. There were different diffraction conditions in the middle and at the edge of wide tunnel. Very dense, three-dimensional dislocation network with some nano-precipitates (less than 50 nm) and cellular dislocation structure are also visible.

At lower cavitation intensity ($J = 5.13$ mW/m^2) the network of very dense, tangled dislocations is still observed, specially along the grain boundaries and in the vicinity of the precipitate (Fig. 14).

Fig. 14. Precipitate and cellular dislocation structure at intensity equal $J = 5.13$ mW/m^2

The density of dislocation at cavitation intensity $J = 5.13$ mW/m^2 (Fig. 14) is clearly lower than that at $J = 10.93$ mW/m^2 (Figs 12, 13). The network of tangled dislocations with nano-metric screw dislocations and nano-precipitates are also observed. Density of the dislocations increased especially along the grain boundaries and at the precipitate. Cellular dislocation structure was also discovered.

At Fig. 15 the black and white "waves" are observed, formed mainly as a result of diffusion of Mg and its subsequent distribution due to the cyclic stress and strain fields. The "waves" propagate through one grain to another. System of dislocations formed cells, low-angle grain boundaries and nano-precipitates occurred. Directive tendency of dislocations is also shown.
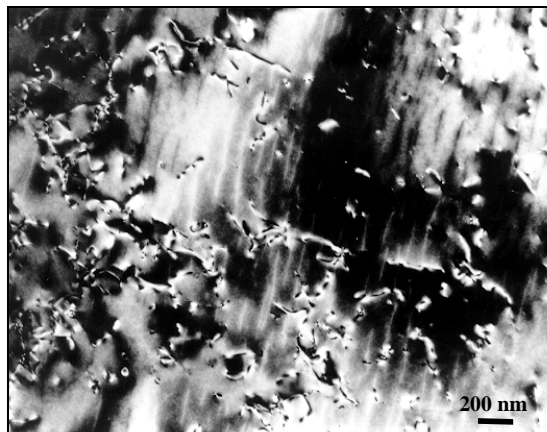
Fig. 15. Nanoprecipitate and waves of diffusion of Mg at the intensity of $J = 5.13$ mW/m^2

The quite different image is observed at very low cavitation intensity $J = 0.026$ mW/m^2 (Fig. 16). The major part of crystal is free of dislocations which appear at boundaries of the precipitates indicating the presence of semi-coherent grain boundaries. The black "waves" and nano-precipitates are also observed.

Fig. 16. Changes in nanostructure at the intensity of J = 0.026 mW/m

DISCUSSION

The relationships between the energy absorbed by eroded material during its exposure, bubble's implosion pressure and the mass loss were indicated in [3,7,16,17]. The mass loss was dependent not only on exposure time but also on a quantity of absorbed energy. Such dependence may explain different cavitation resistance of tested materials.

Presented results of relationship between mass loss in time and cavitation intensity remain in good conformity with previous results [18-22] and measurements of cavitation impulses value [18]. In the high intensity zone $J = 10.93$ mW/m^2 the highest number of high-pressure pulses over 18 MPa measured by 5 mm diameter sensor. In 35 mm distance from barricade (specimen 3) low--pressure pulses predominated. One can suppose, that the high-pressure pulses have fundamental impact on the cavitation erosion progress. As presented in [22], that for aluminium alloy PA2 tested in Erdmann-Jesnitzer' chamber, the correlation between energy flux J density and mass erosion rate existed. It could be described by simple empirical mathematical expression:

$$ER = 1E - 05J^2 + 0,0005J,$$

where:

J   – energy flux density,
ER – cavitation erosion rate.

The results of the experimental investigations of the duration of incubation period (Fig. 4), growth in pits' number formed by collapsing bubbles (Fig. 6), microhardness changes during exposure time (Fig. 9-11) and aluminium alloy dislocations structures (Fig. 12-16) are in good correlation with adopted thesis about relation between cavitation erosion and energy flux density J.

At the zone of high intensity cavitation $J = 10.93$ mW/m^2 the high-pressure pulses of measured values over 7 MPa, predominated. These pulses affect plastic material, as aluminium

alloy and quickly cause dislocation blockade just close to material surface. Cellular dislocation structure and the network of very dense, tangled dislocations, typical of deformation rate, where dislocation can't move occurred (Figs 12, 13). In consequence, high increase of microhardness was observed (Fig. 9). Heat emitted during pulses implosion [2, 6] could cause diffusion of magnesium in aluminium [23] and motion of dislocations in bigger distance from material surface and formation of precipitates and nano-precipitates during cavitation. The gas or steam contained in cavitation babbles has same importance for destruction of the material. It may cause incidental destruction of crystall structure as a result of oxidising (Fig. 12) or hydrogen destruction.

At the zone of middle intensity cavitation ($J = 5.13$ mW/m^2) one can deal with both high--amplitude pulses and low-amplitude pulses. However, the number of latter ones was much greater. Therefore, the existence of cellular dislocation structure caused by high-amplitude pulses can be expected. Besides, there should be found a large number of places where the dislocations were put in motion as a result of low-amplitude action. The alternating field of stresses leads to immobilising of the dislocations and an increase of the density of the fixed dislocations. On the other hand, the heat influence, as well as the change of the stress nature cause the material flow followed by initiation of the stable dislocations movement. It results in the decrease of microhardness both at and beneath the surface of the material (Fig. 9). It is a phenomenon specific of fatigue of the materials. In time, the step by step hardening of the surface layers of the materials subjected to cavitation action is observed – there occurs the mutual blocking of the dislocations, an increase of the retarded dislocations' density and appearance of the cellular structure of dislocations (Figs 14, 15). In deeper layers, the motion of dislocations is more intensive and at simultaneous slight blocking of the same number of dislocations, the slight increase of microhardness occurs (Fig. 9). The density of dislocations in this area is less than density detected at the cavitation intensity of $J = 10.93$ mW/m^2.

At the zone of small intensity ($J = 0.026$ mW/m^2) one deal mainly with low-amplitude pulses. The number of indentations is also much reduced (Fig. 8). The bubble colapses and accompanied heating of the material put the dislocations in motion also in the layers lying deep under the surface [23] of cavitation action. The diffusion of Mg is also observed. As a result, the fall of microhardness on the surface and at 0.2 mm beneath it is detected after 1 minute of cavitation. Further action of cavitation – with the directions of the loading being frequently changed – leads to retarding of the dislocations motion and appearance of low-angle boundaries and precipitates (Fig. 16). It contributes to the low increase of microharness at the surface and in depth of the material (Fig. 11). There appears the state of very strong stresses in the material – which causes the bending of the foil visible in Fig. 5.

CONCLUSIONS

1. The erosion rate increases with increasing energy flux density.
2. The length of incubation period depends on energy flux density J: at $J \leq 1$ mW/m^2 the incubation period is independent of cavitation intensity, and at $J > 1$ mW/m^2 its duration decreases with increasing energy.
3. The pits formed by blowing jet stream have different diameters, and those over 20 μm seem to mainly contribute to the erosion mass loss.
4. The change in microstructure depends on flux density: at high and medium energy the dense, tangled dislocations in the areas of blowing bubbles, at the phase and grain boundaries appear, at also at very low energy some deformation occurs.

REFERENCES

1. Knapp R. T., Daily J. W., Hammit F. G.: *Cavitation.* McGraw-Hill, New York 1970.

2. Brennen Ch. E.: *Cavitation and Buble Dynamics.* Oxford University Press, New York 1995.

3. Steller K.: Res. Rept. Inst. Fluid Machin., Polish Acad. Sci., No. 76, Gdansk 1978.

4. Hucińska J.: *Erozja kawitacyjna w świetle budowy strukturalnej materiałów metalowych.* Ph. D. Thesis, Technical University of Gdańsk, 1976.

5. Heymann F. J., ASTM, No. 408, Atlantic City 1967, p. 70.

6. Tasak E.: *Powierzchniowe zniszczenie i zmiany struktury metali wywołane kawitacyjnym oddziaływaniem cieczy.* Ph. D. Thesis, Acad. Mining Metall., Krakow 1974.

7. Thiruwengadam A. P.: *The concept of erosion strength.* ASTM no. 408, Atlantic City 1966, pp. 22-35.

8. Kirejczyk J.: *Diagnostyka kawitacji w pompach diagonalnych.* Ph. D. Thesis, Inst. Fluid-Flow Machinery PAN, Gdańsk, Poland 1980.

9. Belahadji B., Franc J. P., Michel J. M.: *A statistical analysis of cavitation erosion pits.* Transactions of the ASME, vol. 113, December 1991, pp. 700-706.

10. Hammitt F. H.: *Observations on Cavitatio Damage in a Flowing System.* Journal of Basic Engineering, September 1963, pp. 347-356.

11. Knapp R. T.: *Resent investigations of the mechanics of cavitation and cavitation damage.* Transactions of the ASME, vol. 77. No. 7, October 1055, pp. 1045-1055.

12. Gireń B. G., Szkodo M.: *Size distributions of cavitation pits on laser processed steels.* International Cavitation Erosion Test Seminar, Sopot, Poland 2000, H1-H16.

13. Krella A. Zieliński A.: *Influence of cavitation intensity on erosion of an al-mg alloy.* 9th International Scientific Conference AMME'2000, Sopot, Poland 2000.

14. Norma PN-92/H-93667.

15. Wyrzykowski J. W., Pleszkow E., Sieniawski J.: *Odkształacnie i pękanie metali.* WNT, Warszawa 1999, Poland.

16. Steller J.: *International Cavitation Erosion Test and quantitative assessment of material resistance to cavitation.* WEAR vols. 233-235, pp. 51-64, 1999.

17. Hoff G., Langbein G., Rieger H.: *Material destruction due to liquid impact.* ASTM no. 408, Atlantic City 1966, pp. 42-70.

18. Krella A.: *Badanie wpływu zmian parametrów ruchowych w tunelu kawitacyjnym z komorą typu Erdmanna-Jesnitzera na gęstość strumienia energii doprowadzonej do materiału.* IMP PAN opr. wewn. nr 533/99, Gdańsk 1999.

19. Krella A.: *Wpływ zmiany parametrów ruchowych tunelu kawitacyjnego na zmianę szybkości erozji kawitacyjnej stopu aluminium PA2.* Międzynarodowa konferencja naukowo-techniczna HYDROFORUM, Czorsztyn 18-20 października 2000.

20. Krella A., Zieliński A.: *Wpływ natężenia impulsów kawitacyjnych na krzywe erozji stopu PA2.* I Pomorska konferencja „ Inżynieria Materiałowa", Gdańsk-Sobieszewo'2000.

21. Krella A.: *Invesigations of cavitation erosion of PA2 aluminium alloy.* International Cavitation Erosion Test Seminar, Sopot 1-2nd June 2000, pp. C1-C7.

22. Krella A., Zieliński A., Jezierska E.: *Invesigations of PA2 aluminium alloy of cavitation erosion.* Advanced Materials and Technologies, Gdańsk-Jurata 16-20th September 2001, pp.490-494.

23. Hull D.: Dyslokacje, Warszawa, PWN 1982.